

Maintenance of the International Celestial Reference Frame

S. Lambert, E. F. Arias

SYRTE, Observatoire de Paris, Université PSL, CNRS, Sorbonne Université, LNE
61 av. de l'Observatoire, 75014 Paris, France

Published in IERS annual report 202x

1. The international reference frame ICRF3

Resolution B2 of the XXX IAU General Assembly (IAU 2019) resolves that as from 1 January 2019 ICRF3 is the fundamental realization of the International Celestial Reference System (ICRS). This third representation of the ICRS in radio wavelengths is a catalog of radio source positions described in Charlot et al. (2020) and consists of three catalogs at bands S/X, K and X/Ka with 4536, 824 and 678 objects respectively [<http://iers.obspm.fr/icrs-pc/newwww/icrf>]. Objects in the new frame had been used to orientate the second and third Gaia (Prusti et al. 2016, Brown et al. 2016) data releases DR2 (Brown et al. 2018, Mignard et al. 2018) and EDR3 (Brown et al. 2021, Klioner et al. 2022) catalogs onto the ICRS, as will be the case of the Gaia future catalog releases.

2. Monitoring of the ICRS

Monitoring the ICRS is a mission of the IERS ICRS Centre. With this aim, we perform on a regular basis verification of the stability of the axes of the system materialized through the frame, we characterize the possible deformations of the frame and track the astrometric evolution of its defining sources. Another aspect of this activity consists on the analysis of individual solutions submitted by the VLBI analysis centres to the International VLBI Service (IVS), and their comparison with the international references.

The IERS ICRS Centre at Paris Observatory developed the tools for determining the orientation of the axes, characterizing the deformations of the frame and analyzing the astrometric quality of radio source positions (Lambert 2014). For this report analyses with respect to the conventional reference ICRF3 are presented, as well as with respect to Gaia Early Data Release 3 catalog (EDR3).

3. Analysis of recent VLBI catalogs

3.1. Data

We analyzed five catalogs submitted to the IVS in 2020. The catalogs were respectively computed by the Space Geodesy Centre of the Italian Space Agency (ASI/CGS; solution asi2021a), Geoscience Australia (solutions aus2021a and aus2021b), the German Federal Agency for Cartography and Geodesy (BKG; solution bkg2021a) and Paris Observatory (OP; solution opa2021a). The solutions from ASI, BKG and OPA were obtained with Calc/Solve (Ma et al. 1986). The solutions from AUS were obtained with the OCCAM geodetic VLBI analysis software package (Titov et al. 2004);

The individual frames of all the catalogs had been oriented on ICRF3 by applying no net rotation constraints on ICRF3 defining sources, loose in AUS and OPA solutions. Positions in ICRF3 had been adopted for the a priori catalogs in all the solutions included in this analysis. The two Geoscience Australia catalogs differ only in the data span considered in the solutions, and in consequence the number of sources in the solutions also differs; aus2020b contains about six more months of data. Right ascensions and declinations have been computed as global parameters for most sources. In asi2021a, coordinates of 4791 sources were computed as global parameters, while coordinates of 435 sources were computed as arc-parameters. In solution aus2021a coordinates of 4900 sources with at least four observations were computed as global parameters; coordinates of 49 positionally unstable sources were computed as arc parameters (39 correspond to the special handling sources in ICRF2, 6 objects are unstable AGNs and 4 are radio stars). 5197 source coordinates were computed as global parameters in solution aus2021b, and 54 sources positionally unstable (including 50 AGNs) were computed as arc-parameters. All source coordinates in opa2021a were computed as global parameters, with the exception of 6 radio stars and 7 known gravitational lenses. The galactocentric aberration has been corrected in all solutions according to MacMillan (2019), and the recommendation of the IVS Working Group on Galactic Aberration.

In our analysis we have compared these individual solutions to the catalog representing ICRF3 in the S/X bands (ICRF3X in this report) and to the catalogue resulting from the Gaia Early Data Release 3 (EDR3, Prusti et al. 2016, Brown et al. 2021).

3.2. Overview of the catalogs

The number of sources in each catalog, the mean epoch of the observations, and the median positional errors (for RA cos DEC, Dec, and for the error ellipse major axis) are reported in Table 1. The standard error of the catalog positions differs in the solutions. AUS positions might be influenced by a large number of sources with errors in the range 0.6 – 1 mas in the Southern hemisphere. These features are visible in the plots of Fig. 1.

The sky distribution of the radio sources in each catalog is plotted in Fig. 1 together with the distribution of the standard errors. In the sky maps, the color indicates the overall error computed as the major axis of the error ellipse, calculated using the correlation information between the coordinates as provided in the catalogs.

Table 1. *Statistic information of the catalogs here reported. N is the number of sources. The mean epoch corresponds to the average of the mean observational epochs of each source. N is the number of sources, E_RA*, E_Dec are respectively the median standard errors in right ascension (scaled by cos dec) and in declination, E_EEMA is the median major axis of error ellipses. Unit is μ as.*

	N	Epoch	E_RA*	E_Dec	E_EEMA
opa2021a	5117	2015.52	110.03	190.63	194.75
asi2021a	4791	2015.49	104.82	180.12	183.09
aus2021a	4900	2015.35	225.53	455.34	461.86
aus2021b	5197	2015.73	221.25	448.45	454.58
bkg2021a	4673	2014.19	152.70	267.04	276.67

IERS Annual Report 2021

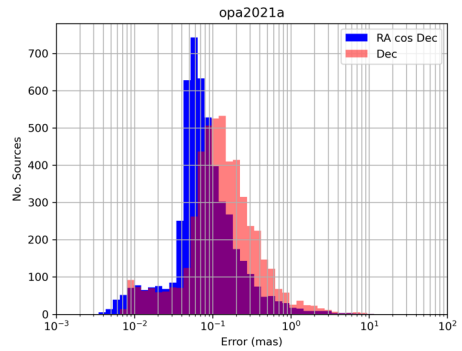
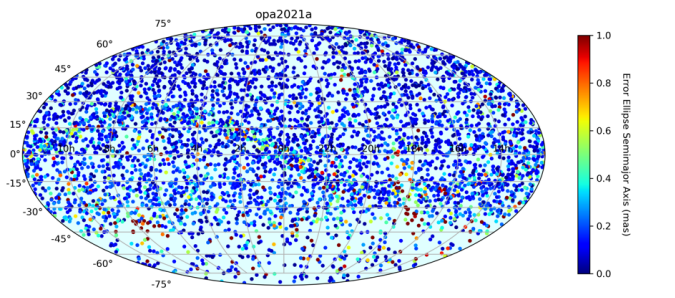
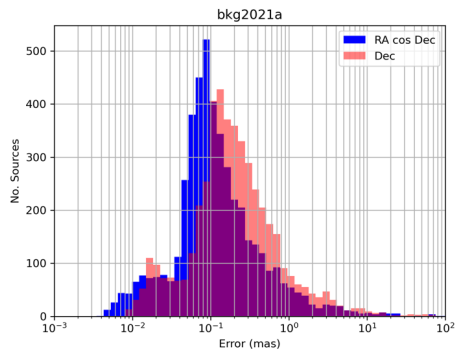
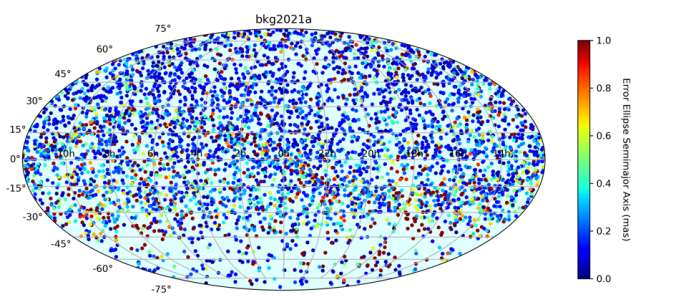
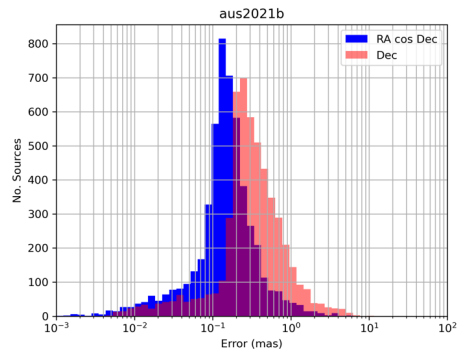
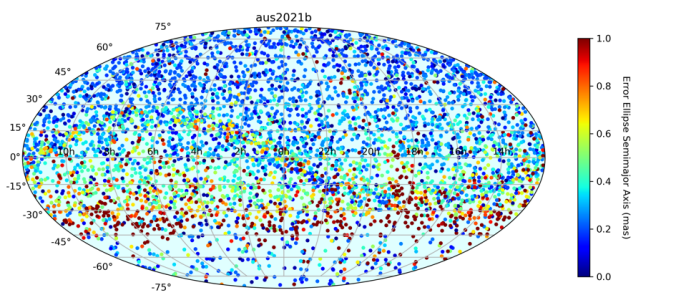
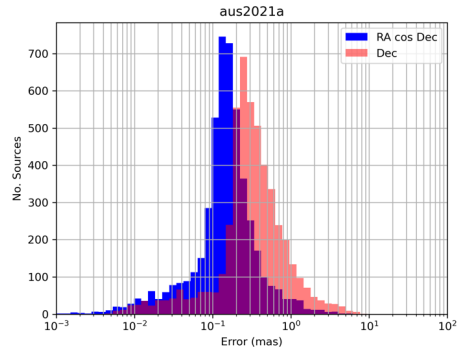
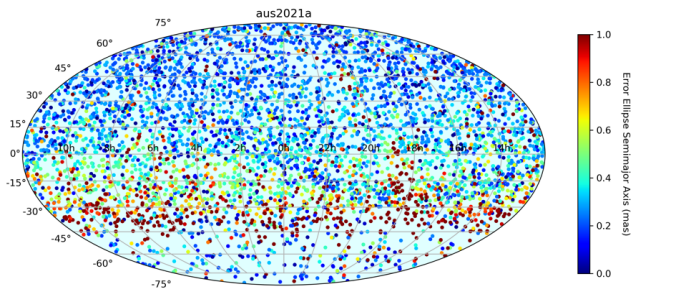
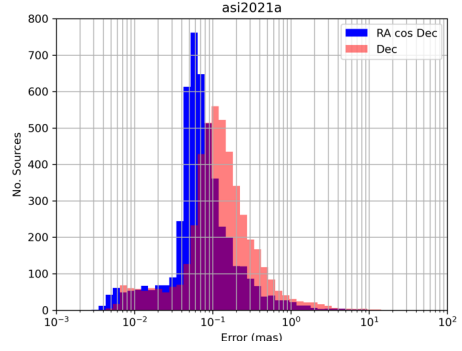
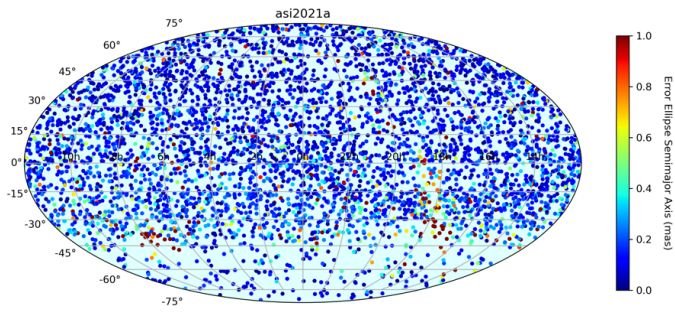


Figure 1 – Previous page. *Left: sky distribution of the catalogs highlighting the overall positional error computed as the major axis of the error ellipse. Right: distribution of the standard errors on source position.*

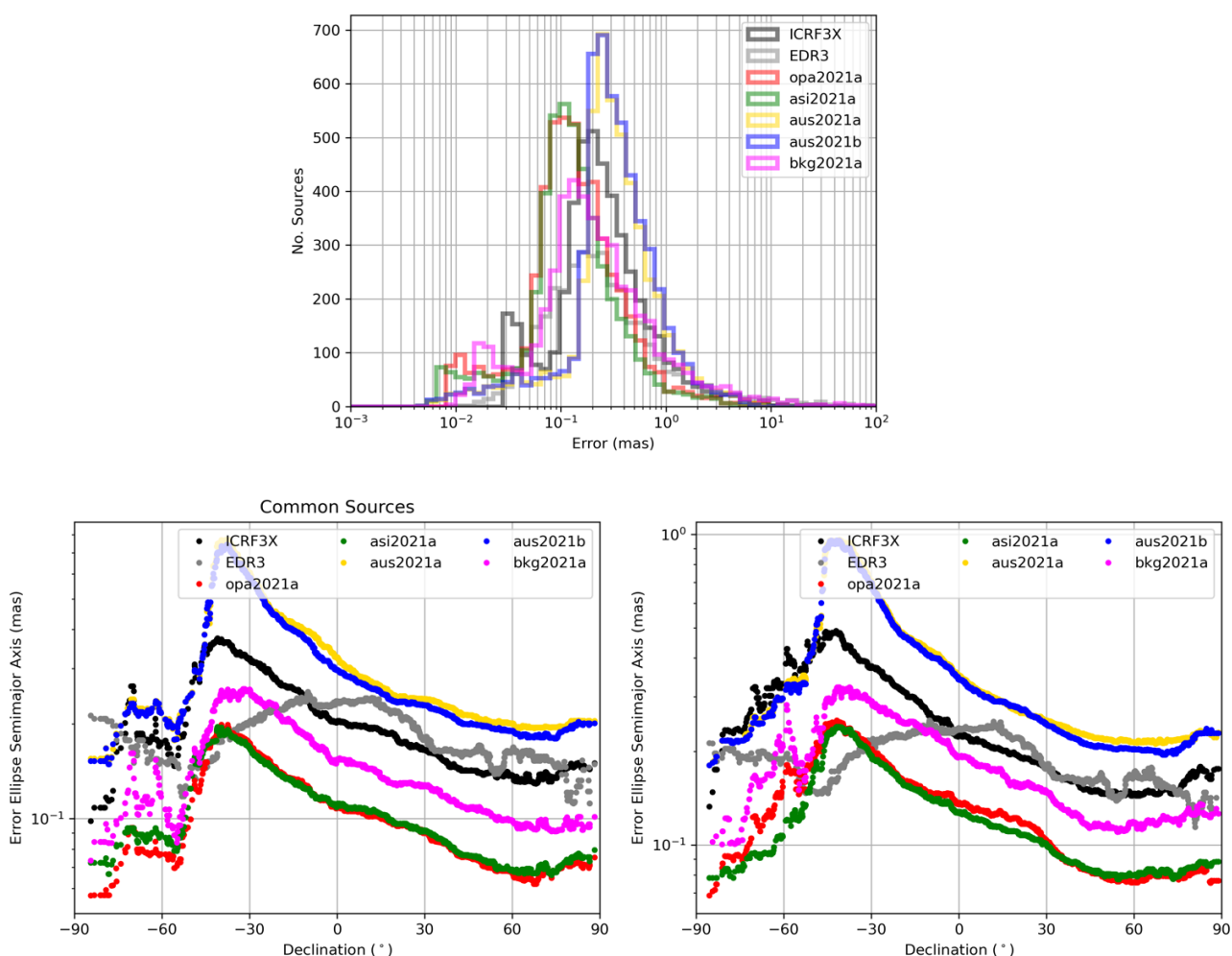


Figure 2. *Top: overall comparison of the standard error distribution. Bottom: standard errors in source positions as a function of the declination smoothed by taking the running median within bins of 15 degrees, for sources common to all catalogs (left) and for all sources in each catalog (right).*

Fig. 2 presents three plots; at the top the error distribution, including that of the catalogs used as reference in the comparisons (ICRF3X and Gaia EDR3); at the bottom the dependence of the error on the declination including the common sources to all catalogs (left) and all sources in each catalog (right) are displayed for which we took the running median error within windows of 15°.

The plots show a clear declination-dependent error for the individual catalogs. When sources common to all catalogs are considered, the behavior of the VLBI solutions is similar, peaking at about -40° declination, and reaching small error values around $+60^\circ$ declination, certainly due to the presence of a substantial number of good astrometric common sources in that region. This effect remains visible in the plot where all sources in each catalog are considered, where errors are slightly larger. AUS solutions show large errors at mid-latitudes in the Southern hemisphere, very probably due to the network asymmetry and the quality of the sources in the South, visible in Fig. 1. The Gaia scanning law allows to cover both hemispheres symmetrically, and in consequence the Gaia EDR3 catalog does not show such systematic effects, as ICRF3 does.

3.3. Comparison with ICRF3 and Gaia EDR3

Figure 3 displays the differences in declination between the catalogs and the references averaged within bins of 200 sources in two configurations: all sources (left) and sources common to all catalogs (right). In the comparison with ICRF3X, all sources, the asi2020a is rather smooth, with a small deformation of about $30 \mu\text{as}$ at -30° declination; deformations of the AUS solutions are small at positive declinations, but peak about $-70 \mu\text{as}$ and $-60 \mu\text{as}$ between at Southern declinations, probably due to the network geometry and the quality of sources at negative declinations. The OP solution shows a significant deformation of about $50 \mu\text{as}$ between 0° and $+45^\circ$ declination; the BKG solution shows deformations with a peak of about $-60 \mu\text{as}$ on the equator. Deformations are smoother when the differences are computed with common sources (top right). The amplitude of the deformations is bigger when the differences are computed with respect to Gaia EDR3, since the sphere of Gaia is in principle not affected by deformations.

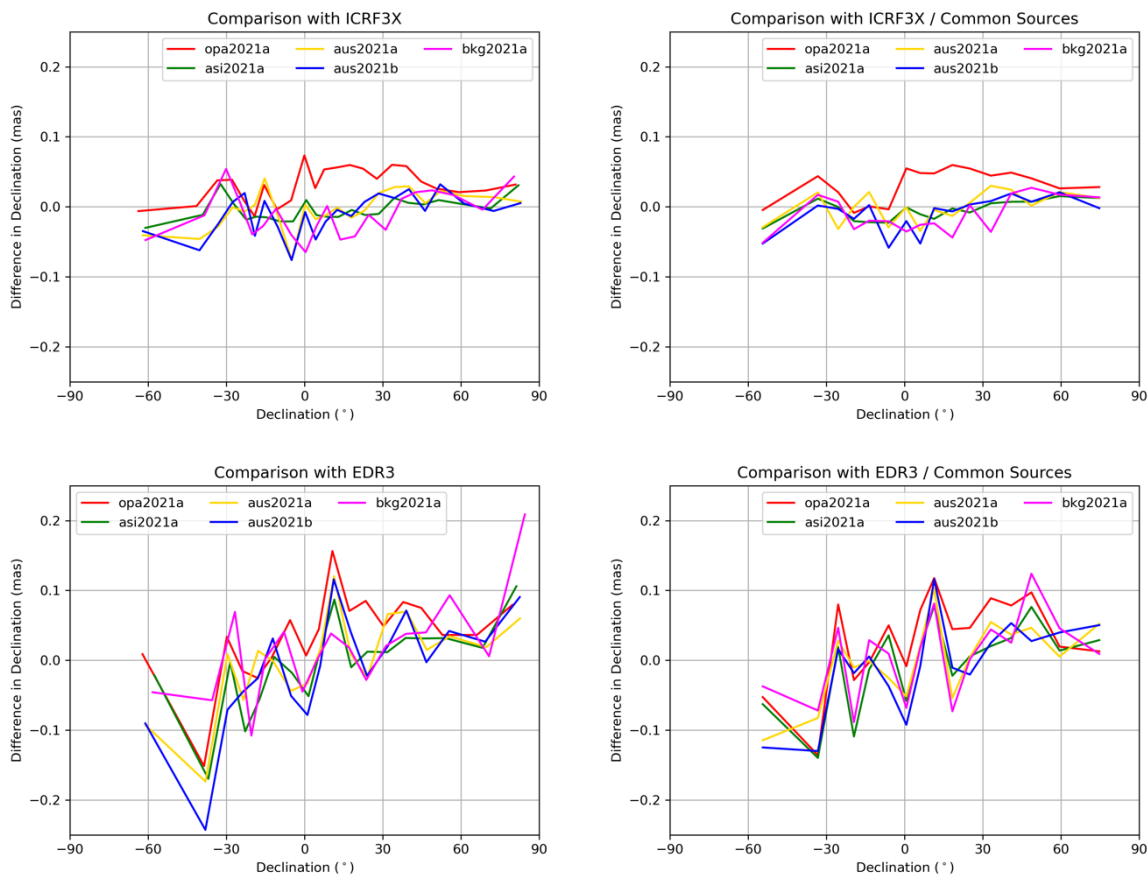


Figure 3. Differences in declination between the catalogs and the references (ICRF3X: top; Gaia EDR3, bottom) averaged in bins of 200 sources sorted by declination for all sources (left) and for common sources to all catalogs (right).

Catalog comparisons had been computed using the 16-parameter transformation accounting for rotations around the three axes, a glide, and degree-2 electric- and magnetic-type deformations (see e.g., Mignard and Klioner 2012) together with an outlier elimination process preliminary to the fit as described in Charlot et al. (2020). The coordinate differences $\Delta\alpha$ and $\Delta\delta$ between a catalog and a reference catalog read

$$\begin{aligned}
 \Delta\alpha \cos \delta &= R_1 \cos \alpha \sin \delta + R_2 \sin \alpha \sin \delta - R_3 \cos \delta - D_1 \sin \alpha + D_2 \cos \alpha + M_{20} \sin 2\delta \\
 &+ (E_{21}^{\text{Re}} \sin \alpha + E_{21}^{\text{Im}} \cos \alpha) \sin \delta - (M_{21}^{\text{Re}} \cos \alpha - M_{21}^{\text{Im}} \sin \alpha) \cos 2\delta \\
 &- 2 (E_{22}^{\text{Re}} \sin 2\alpha + E_{22}^{\text{Im}} \cos 2\alpha) \cos \delta - (M_{22}^{\text{Re}} \cos 2\alpha - M_{22}^{\text{Im}} \sin 2\alpha) \sin 2\delta, \\
 \Delta\delta &= -R_1 \sin \alpha + R_2 \cos \alpha - D_1 \cos \alpha \sin \delta - D_2 \sin \alpha \sin \delta + D_3 \cos \delta + E_{20} \sin 2\delta \\
 &- (E_{21}^{\text{Re}} \cos \alpha - E_{21}^{\text{Im}} \sin \alpha) \cos 2\delta - (M_{21}^{\text{Re}} \sin \alpha + M_{21}^{\text{Im}} \cos \alpha) \sin \delta \\
 &- (E_{22}^{\text{Re}} \cos 2\alpha - E_{22}^{\text{Im}} \sin 2\alpha) \sin 2\delta + 2 (M_{22}^{\text{Re}} \sin 2\alpha + M_{22}^{\text{Im}} \cos 2\alpha) \cos \delta,
 \end{aligned}$$

where α and δ are the coordinates of the object in the reference catalog. We used weighted least-squares to solve the system, with weights computed using the available covariance information (i.e., the standard errors on individual source coordinates and their correlation). The values of the transformation parameters adjusted to the catalogs compared to the ICRF3X and Gaia EDR3 and their standard errors are reported in Fig. 4 for two different set of sources, those common to all catalogs and each reference, and those common between each catalog and the reference. The resulting statistics after removal of systematics are reported in Table 2. Fig. 4 reveals that the results are similar independently from the set of sources used for the comparisons. The comparisons with ICRF3X show significant rotation parameters for OP and BKG solutions, where y-axis misalignment reach some 50 μs for OP and 70 μs for BKG. OP has a visible deformation through the glide parameters. The rotation effects are also visible when Gaia EDR3 is the reference, since it has been oriented onto ICRF3. Deformations are visible dependent on declination, consistently with Fig. 2.

Table 2. Statistics of the differences of the catalogs to ICRF3X and Gaia EDR3 with different sets of common sources, and after removal of large-scale systematics. RA* stands for RA cos_dec. Unit is μs .

2a. With respect to ICRF3X, N: number of sources common to ICRF3X and each individual catalog.										
	N	Std_RA*	Std_Dec	Chi2_RA*	Chi2_Dec	Std_RA*	Std_Dec	Chi2_RA*	Chi2_Dec	
opa2021a	4490	88.05	101.96	0.63	0.56	81.85	93.13	0.54	0.47	
asi2021a	4478	74.86	88.59	0.46	0.44	74.08	86.72	0.45	0.42	
aus2021a	4452	125.32	136.55	0.81	0.59	125.19	135.75	0.80	0.59	
aus2021b	4456	122.34	136.54	0.79	0.61	122.23	135.46	0.79	0.60	
bkg2021a	4105	110.57	135.96	0.94	0.93	106.30	124.20	0.87	0.78	
2b. With respect to ICRF3X, N: number of sources common to all catalogs.										
	N	Std_RA*	Std_Dec	Chi2_RA*	Chi2_Dec	Std_RA*	Std_Dec	Chi2_RA*	Chi2_Dec	
opa2021a	3150	81.48	95.04	0.63	0.58	74.88	85.03	0.53	0.46	
asi2021a	3150	68.41	80.91	0.45	0.43	67.63	79.06	0.44	0.41	
aus2021a	3151	111.83	118.27	0.79	0.57	111.68	117.38	0.79	0.56	
aus2021b	3150	109.02	117.51	0.77	0.57	108.86	116.38	0.77	0.56	
bkg2021a	3150	100.64	126.14	0.89	0.93	96.04	113.41	0.81	0.75	
2c. With respect to Gaia-EDR3, N: number of sources common to EDR3 and each individual catalog.										
	N	Std_RA*	Std_Dec	Chi2_RA*	Chi2_Dec	Std_RA*	Std_Dec	Chi2_RA*	Chi2_Dec	
opa2021a	3490	252.45	270.87	3.03	2.09	250.81	266.16	2.99	2.01	
asi2021a	3473	250.01	265.25	3.01	2.05	248.55	263.15	2.97	2.02	
aus2021a	3446	309.36	322.58	3.49	1.52	308.18	320.37	3.47	1.50	
aus2021b	3450	298.00	321.87	3.35	1.56	296.93	319.15	3.33	1.53	
bkg2021a	3218	265.87	293.09	2.88	2.13	264.15	288.52	2.84	2.06	
2d. With respect to Gaia-EDR3, N: number of sources common to all catalogs.										
	N	Std_RA*	Std_Dec	Chi2_RA*	Chi2_Dec	Std_RA*	Std_Dec	Chi2_RA*	Chi2_Dec	
opa2021a	3150	248.81	268.91	3.00	2.12	247.36	263.74	2.97	2.04	
asi2021a	3150	246.54	263.11	2.96	2.06	245.02	260.67	2.93	2.02	
aus2021a	3151	299.08	314.25	3.37	1.53	298.01	311.81	3.34	1.51	
aus2021b	3150	290.80	313.73	3.27	1.56	289.80	310.79	3.24	1.53	
bkg2021a	3150	265.35	292.81	2.87	2.12	263.42	288.20	2.83	2.06	

Galactic aberration has been accounted for at the construction of ICRF3. Uncorrected Galactic aberration should provoke a glide of amplitude close to $5 \mu\text{as/yr}$ (e.g., Kovalevsky 2003; Titov et al. 2011) towards the Galactic center (approx. R.A. 265° and declination -29°). A value of $5.8 \mu\text{as/yr}$ for the amplitude of the Galactic aberration has been evaluated in analyses performed at the construction of the ICRF3 (MacMillan et al. 2019). The descriptions of the catalogs provided to the IVS used in this report indicate that this correction has been applied in the solutions (for details refer to <http://ivsopar.obspm.fr/vlbi/ivsproducts/crf/>).

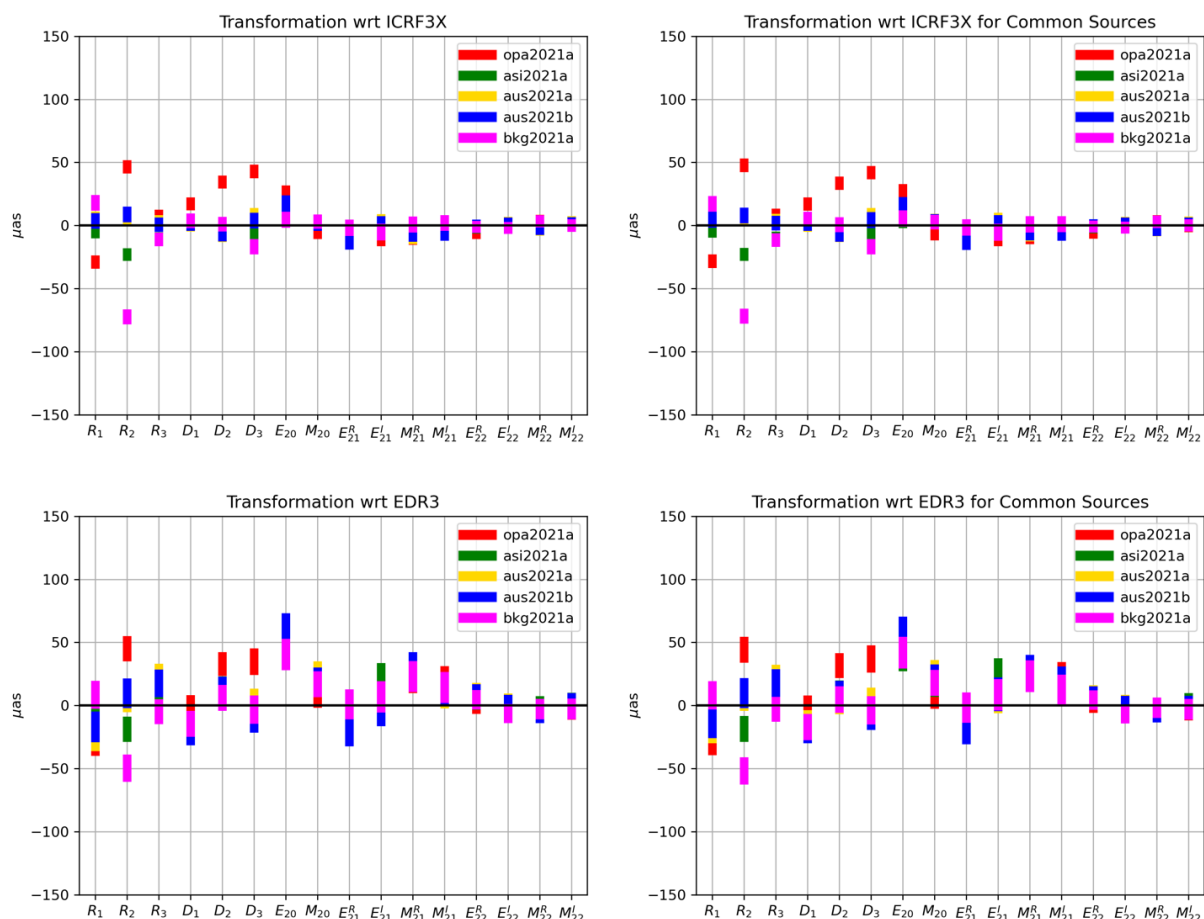


Figure 4. Transformation parameters between the catalogs under analysis and the reference frames (ICRF3X: top, Gaia EDR3: bottom). The plots on the left represent parameters computed with sources common to each individual catalog and the frame used as reference (from top to bottom they correspond to the statistics in tables 2a and 2c); the plots on the right represent parameters computed with sources common to all the catalogs involved in the comparisons, including the references (from top to bottom they correspond to the statistics in tables 2b and 2d).

3.4. Conclusions and recommendations

Five individual catalogs from four analysis centres submitted to the IVS in 2021 are analyzed in this report. The axes of their frames are consistent with ICRF3X at the level of $10 \mu\text{as}$ for most solutions, with misalignments of $50 - 70 \mu\text{as}$ in two cases (OP and BKG). Zonal deformations remain beyond $20 \mu\text{as}$, except for the OP solution. Similar results for the rotations are obtained in the comparisons with Gaia EDR3, and significant zonal deformations.

In all solutions the correction for the amplitude of the Galactic aberration has been implemented using the recommended value. The catalogs should be as complete as possible, i.e., processing as much VLBI sessions as possible since 1979. Analysis strategies should be rigorously documented and motivated. The main points that will be scrutinized in the next reports will be the zonal systematics, their relation with the Galactic aberration, and the agreement with the current (EDR3) and future releases of Gaia.

4. References

A. G. A. Brown, A. Vallenari, T. Prusti, J. H. J. de Bruijne, et al. Gaia Data Release 1. Summary of the astrometric, photometric, and survey properties. *Astronomy & Astrophysics*, 595:A2, Nov. 2016.

A. G. A. Brown, A. Vallenari, T. Prusti, J. H. J. de Bruijne, et al. Gaia Data Release 2. Summary of the contents and survey properties. *Astronomy & Astrophysics*, 616:A1, Aug. 2018.

A. G. A. Brown, A. Vallenari, T. Prusti, J. H. J. de Bruijne, et al. Gaia Early Data Release 3. Summary of the contents and survey properties. *Astronomy & Astrophysics*, 649:A1, 2021.

P. Charlot, C. S. Jacobs, D. Gordon, S. B. Lambert, A. de Witt, J. Boehm, A. L. Fey, R. Heinkelmann, E. Skurikhina, O. Titov, E. F. Arias, S. Bolotin, G. Bourda, C. Ma, Z. Malkin, A. Nothnagel, D. Mayer, D. S. MacMillan, T. Nilsson and R. Gaume, The third realization of the International Celestial Reference Frame by very long baseline interferometry. *Astronomy & Astrophysics*, 644, A159, Dec. 2020.

International Astronomical Union. Transactions IAU, Vol. XXXB, Proc. of the XXX IAU General Assembly, August 2018 (Ed. Teresa Lago), 2019.

S. A. Klioner, L. Lindegren, F. Mignard, J. Hernandez, et al. Gaia Early Data Release 3. The celestial reference frame (Gaia-CRF3). *Astronomy & Astrophysics*, 2022.

J. Kovalevsky. Aberration in proper motions. *Astronomy & Astrophysics*, 404:743–747, June 2003.

S. Lambert. Comparison of VLBI radio source catalogs. *Astronomy & Astrophysics*, 570:A108, 2014

C. Ma, T. A. Clark, J. W. Ryan, T. A. Herring, I. I. Shapiro, B. E. Corey, H. F. Hinteregger, A. E. E. Rogers, A. R. Whitney, C. A. Knight, G. L. Lundqvist, D. B. Shaffer, N. R. Vandenberg, J. C. Pigg, B. R. Schupler, and B. O. Ronnang. Radio-source positions from VLBI. *Astronomical Journal*, 92:1020–1029, Nov. 1986.

D. S. MacMillan, A. L. Fey, J. M. Gipson, D. Gordon, C. S. Jacobs, H. Krásná, S. Lambert, Z. Malkin, O. A. Titov, G. Wang, and M. H. Xu, Galactocentric acceleration in VLBI analysis - Findings of IVS WG8, *Astronomy and Astrophysics*, 630:A93, 2019

F. Mignard and S. Klioner. Analysis of astrometric catalogues with vector spherical harmonics. *Astronomy & Astrophysics*, 547:A59, 2012.

F. Mignard, S. A. Klioner, L. Lindegren, J. Hernandez, U. Bastian, A. Bombrun, D. Hobbs, U. Lammers, D. Michalik, and et al. Gaia Data Release 2. The celestial reference frame (Gaia-CRF2). *Astronomy & Astrophysics*, 616:A14, 2018.

T. Prusti, J. H. J. de Bruijne, A. G. A. Brown, Vallenari, A., Babusiaux, C., Bailer-Jones, C. A. L., Bastian, U., Biermann, M., Evans, D. W., and et al. The Gaia mission. *Astronomy & Astrophysics*, 595:A1, 2016.

O. Titov, V. Tesmer, and J. Boehm. OCCAM v.6.0 Software for VLBI Data Analysis. In N. R. Vandenberg and K. D. Baver, editors, *International VLBI Service for Geodesy and Astrometry 2004 General Meeting Proceedings*, page 267, June 2004.

O. Titov, S. B. Lambert, and A.-M. Gontier. VLBI measurement of the secular aberration drift. *Astronomy & Astrophysics*, 529:A91, May 2011.